UCSF
UC San Francisco Previously Published Works

Title
In-polar InN grown by plasma-assisted molecular beam epitaxy

Permalink
https://escholarship.org/uc/item/1sn109sc

Journal
Applied Physics Letters, 89(3)

ISSN
0003-6951

Authors
Gallinat, C S
Koblmuller, G
Brown, J S
et al.

Publication Date
2006-07-01

Peer reviewed

eScholarship.org Powered by the California Digital Library
University of California

In-polar InN grown by plasma-assisted molecular beam epitaxy

Chad S. Gallinat,[a] Gregor Koblmüller, Jay S. Brown,
Sarah Bernardis, and James S. Speck
Materials Department, University of California, Santa Barbara, California 93106-5050

Grace D. Chern, Eric D. Readinger, Hongen Shen, and Michael Wraback
U.S. Army Research Laboratory, Sensors and Electron Devices Directorate, 2800 Powder Mill Road, Adelphi, Maryland 20783

(Received 29 March 2006; accepted 25 May 2006; published online 20 July 2006)

We study the effect of different deposition conditions on the properties of In-polar InN grown by plasma-assisted molecular beam epitaxy. GaN buffer layers grown in the Ga-droplet regime prior to the InN deposition significantly improved the surface morphology of InN films grown with excess In flux. Using this approach, In-polar InN films have been realized with room temperature electron mobilities as high as $2250\ \mathrm{cm^2/V\ s}$. We correlate electron concentrations in our InN films with the unintentionally incorporated impurities, oxygen and hydrogen. A surface electron accumulation layer of $5.11\times10^{13}\ \mathrm{cm^{-2}}$ is measured for In-polar InN. Analysis of optical absorption data provides a band gap energy of ~0.65 eV for the thickest InN films. © *2006 American Institute of Physics*.
[DOI: 10.1063/1.2234274]

Recent advances in III-nitride deposition techniques have facilitated the growth of high quality InN films and established an updated band gap value of 0.67–0.8 eV.[1–4] This smaller band gap value has opened the III-nitride system to unique possible electronic and optoelectronic applications. However, the electrical properties of InN are still a source of dispute due to the high unintentionally doped electron concentrations.[5–8] Recent theoretical calculations predict an ultimate room temperature electron mobility for InN to reach $14\,000\ \mathrm{cm^2/V\ s}$.[9] Based on this prediction and the flurry of recent activity, there appears to be room for improvement in the growth of InN.

In this letter, we present optimized In-polar InN grown by plasma-assisted molecular beam epitaxy (PA-MBE). Our approach for this study was to create a growth diagram for In-polar InN similar to what has been developed for the PA-MBE growth of Ga-polar GaN,[10,11] understand the effect of a GaN buffer layer, and begin to explore the origin of InN's electrical properties. The samples presented here were grown in a Varian/EPI 620 chamber with conventional Knudsen cells for group III sources and an EPI Unibulb radio frequency plasma source for the active nitrogen species. We document all fluxes in terms of growth rate (nm/min) as calibrated by thickness measurements of In-rich and N-rich InN samples. An Ircon Modline 3 pyrometer was employed to measure the growth temperature. All of the samples presented here were grown on semi-insulating (Fe-doped) Ga-polar GaN templates provided by Lumilog. Reflection high energy electron diffraction (RHEED) was used to monitor the growth mode and metal coverage *in situ*. The samples were characterized *ex situ* by optical microscopy, atomic force microscopy (AFM), room temperature Hall effect measurements, and high-resolution x-ray diffraction (HRXRD). To analyze unintentionally incorporated impurities, secondary ion mass spectrometry (SIMS) measurements were performed using implant standards for the quantification of hydrogen and oxygen.

[a]Electronic mail: chadsg@engineering.ucsb.edu

The initial approach in developing an In-polar InN growth diagram was to identify a temperature window necessary for growth. Figure 1(a) shows the relatively simple InN growth diagram—the details of the construction of this diagram will be published elsewhere. It was observed that at temperatures above 500 °C there was no InN growth and only In metal was deposited onto the substrate, regardless of the In flux/active nitrogen ratio. Growth of In-polar InN should be possible beyond 500 °C, however, with an appropriate increase in active nitrogen to offset InN dissociation. At growth temperatures between 420 and 490 °C fully coalesced InN layers were realized.

Based on this growth temperature window, a series of samples were grown, varying only the In flux (from as high as ~17 nm/min to as low as ~3 nm/min)—keeping the substrate temperature and the active nitrogen constant (450 °C and 12 nm/min, respectively). Two growth regimes were identified, as characterized by surface morphology (by AFM): the N-rich regime [Fig. 1(c)] and the In-droplet regime [Fig. 1(b)]. This observation is different from GaN in which three growth regimes are identified for the PA-MBE growth in the metal-polar orientation.[10,11] This two-regime growth behavior persists for all substrate temperatures at which InN films were realized.

Upon completion of the growth diagram, we turned our attention to optimizing a buffer layer to precede InN growth. Reports of using an AlN buffer layer on sapphire,[12] a low-temperature InN buffer layer on sapphire,[13] a double buffer

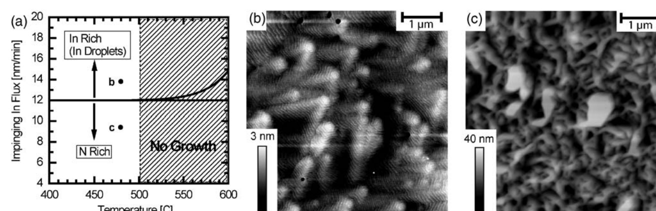

FIG. 1. (a) In-polar InN PA-MBE growth diagram and AFM micrographs of (b) a 1.5 μm thick InN layer grown in the In-droplet regime and (c) a 1 μm thick InN layer grown in the N-rich regime.

 © 2006 American Institute of Physics
Downloaded 23 Jul 2006 to 128.111.179.10. Redistribution subject to AIP license or copyright, see http://apl.aip.org/apl/copyright.jsp

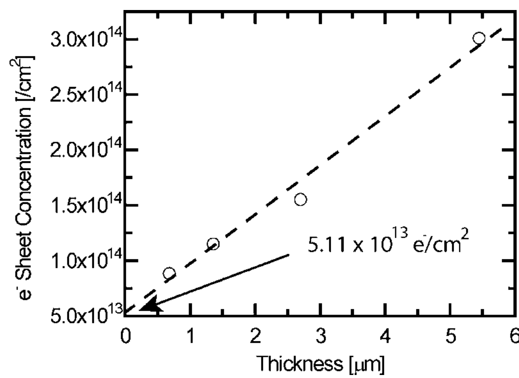

FIG. 2. Dependence of the electron sheet concentration on InN film thickness.

utilizing Si_3N_4/AlN on Si,[14] and a GaN buffer on sapphire[15] have all improved the structural and electrical properties of InN. Growth on GaN templates provide yet another substrate for the PA-MBE growth of InN, and optimization of a GaN buffer layer is a necessary step for improving the quality of InN.

Initial In-polar InN epilayers were grown directly on the GaN templates. This resulted in InN layers that were not fully coalesced and exhibited many surface pits as observed by AFM; therefore, it was necessary to optimize the buffer layer to precede InN growth. According to the GaN growth diagram,[10,11] we grew GaN buffer layers in the three different GaN growth regimes (N-rich, intermediate Ga-rich, and Ga-droplet Ga-rich). It was found that In-rich InN layers grown on 100 nm thick N-rich and intermediate grown GaN buffer layers were delaminated from the underlying buffer layer. GaN buffer layers were grown in the Ga-droplet growth regime required complete desorption of excess Ga from the surface before starting InN growth. This was achieved by choosing a high enough substrate temperature (700 °C) and monitoring the increase in RHEED intensity to the pregrowth value. RHEED intensities of low contrast are typically associated with the presence of metallic droplets, while increased RHEED intensity indicates metal desorption.[16] After complete Ga desorption, subsequent InN layers were grown at varying growth temperatures, In fluxes, and plasma conditions. InN layers grown on GaN buffer layers grown in the Ga-droplet regime adhered entirely to the underlying layer with no blistering or delamination. InN layers grown on this optimized buffer layer [Fig. 1(b)] had smoother surface morphologies and less surface pitting as compared to layers grown directly on the GaN template or to those grown in the N-rich regime [Fig. 1(c)].

It has been reported that there exists a large density of electrons at the InN surface (2.5×10^{13} cm^{-2}).[17,18] To evaluate the surface electron accumulation in our optimized In-polar InN, we grew a series of samples at differing thicknesses, measured the Hall sheet carrier concentration, and extrapolated the fitted curve to zero film thickness (Fig. 2). The surface electron density determined from the fit was 5.11×10^{13} cm^{-2}, while the bulk electron density was 4.46×10^{17} cm^{-3}. Throughout this letter, the surface electron density was subtracted from the measured electron concentration to provide a more accurate bulk electron concentration.

The origin of the high electron concentrations in InN was explored using SIMS. Electronic structure calculations

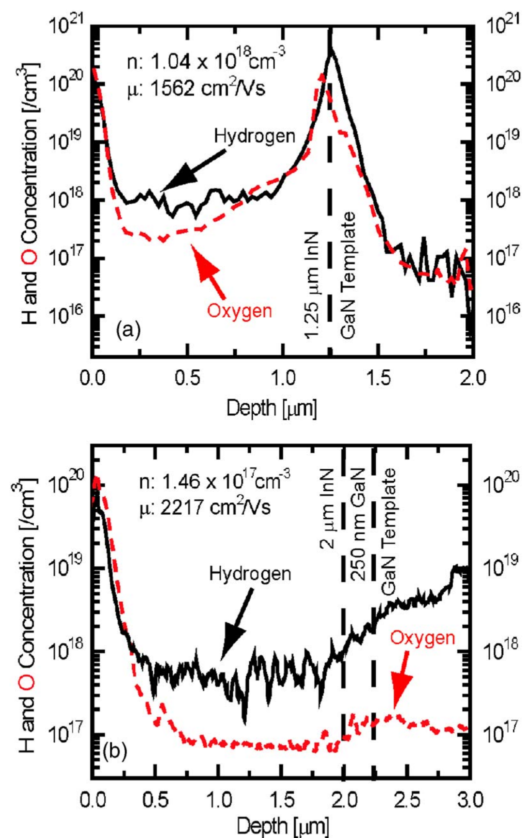

FIG. 3. (Color online) SIMS profiles quantifying the unintentionally incorporated impurities, hydrogen (solid line) and oxygen (dashed line), in (a) a 1.25 μm thick InN sample grown directly on a GaN template and (b) a 2 μm InN sample grown on a 250 nm thick Ga-droplet GaN buffer layer.

predict that both hydrogen and oxygen are shallow donors in InN.[19,20] Using these predictions as a guide, both oxygen and hydrogen levels were quantified in representative samples. Figure 3 shows SIMS profiles for two different samples grown at a substrate temperature of 450 °C in the In-droplet regime: (a) a 1.25 μm InN film grown directly on a GaN template and (b) a 2 μm InN film grown on a 250 nm thick Ga-droplet GaN buffer. For the sample shown in Fig. 3(a), the average hydrogen concentration in the InN layer was 1.11×10^{18} cm^{-3} and the average oxygen concentration was 7.69×10^{17} cm^{-3}. Hall measurements on the same sample yielded a bulk electron concentration of 1.04×10^{18} cm^{-3} and a mobility of 1562 cm^2/V s. The InN layer in Fig. 3(b) exhibited a smaller average hydrogen concentration (5.72×10^{17} cm^{-3}) and a smaller oxygen concentration (8.75×10^{16} cm^{-3}) through the bulk of the InN layer. This layer also had a lower measured electron concentration (1.46×10^{17} cm^{-3}) and a higher mobility (2217 cm^2/V s) than the sample grown directly on the GaN template. In both samples the hydrogen levels in the InN layer were comparable to the free electron concentrations—suggesting that hydrogen was the dominant unintentional impurity donor in these films.

Overall, samples grown directly on the GaN templates had on average higher electron carrier concentrations (4.71×10^{17}–1.04×10^{19} cm^{-3}) and lower electron mobilities (1575–1290 cm^2/V s) as compared to samples grown using a Ga-droplet GaN buffer layer (3.5×10^{17}–7.75×10^{17} cm^{-3} and 2250–1606 cm^2/V s).

Downloaded 23 Jul 2006 to 128.111.179.10. Redistribution subject to AIP license or copyright, see http://apl.aip.org/apl/copyright.jsp

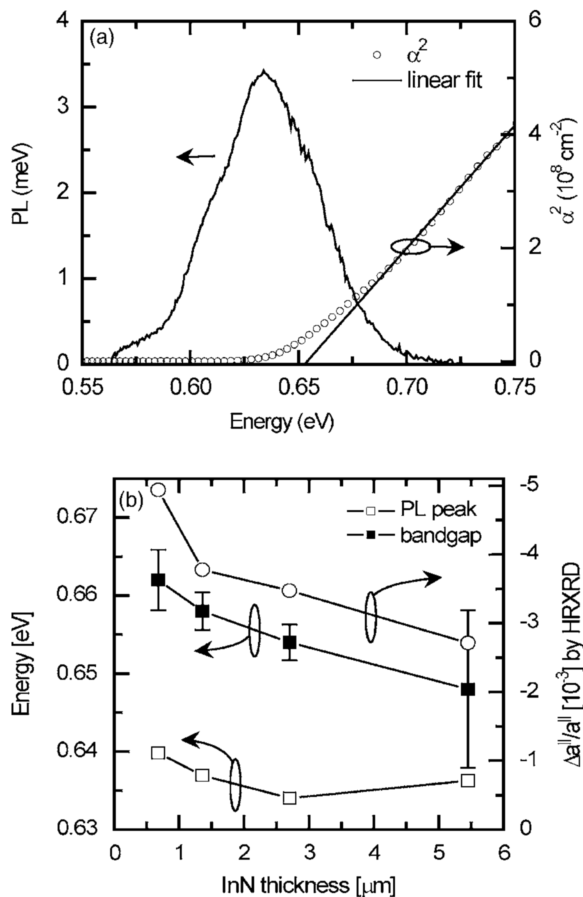

FIG. 4. (a) Band gap obtained from absorption data and PL spectrum from the 2.7 μm InN sample; (b) comparison of band gap energy, peak PL emission energy, and residual compressive strain as a function of InN thickness.

With a value of 2250 cm^2/V s, we report one of the highest measured RT electron mobilities for In-polar InN.

The optical properties of the InN thickness series were evaluated at room temperature by cw reflectance, transmission, and photoluminescence (PL) measurements. The absorption coefficient was calculated from the reflectance and transmission data, and its square is plotted versus photon energy to determine the direct band gap of the InN. Figure 4(a) shows representative results for the 2.7 μm thick sample. The intercept of the linear fit with the energy axis provides a band gap of 0.654 ± 0.002 eV. The PL peak was Stokes shifted from 20 meV to 0.634 eV, implying that the emission emanates substantially from the bandtail states. Figure 4(b) compares the band gap obtained from the fit described above, the PL peak energy, and the residual compressive strain (as measured by HRXRD) for the InN film thickness series. The band gap decreased from 0.662 ± 0.004 to 0.648 ± 0.01 eV as the film thickness increased from 0.68 to 5.45 μm, most likely due to the reduction in residual compressive strain. Comparison of the shift in band gap with variation in compressive strain allows us to estimate the deformation potential for wurtzite InN to be 5.0 eV, a higher value than what was expected according to theoretical calculations (4.2 eV).[21] Extrapolation to zero strain using the experimentally determined deformation potential (5.0 eV) yields a band gap value of 0.63 ± 0.007 eV. A similar shift in PL peak energy, from 0.64 to ~ 0.635 eV, was observed with increasing film thickness. This wavelength shift may be less pronounced because the absorption depth of the 900 nm excitation laser is much smaller ($\sim$200–300 nm) than the thickness of most of the InN films.

In summary, the presence of a GaN buffer layer grown in the Ga-droplet regime was necessary for the highest quality InN films. We have measured amongst the highest RT electron mobility for In-polar InN (2250 cm^2/V s) and found a direct correlation between the free electron concentration in InN and the incorporation of hydrogen and oxygen. We measured an electron accumulation layer of 5.11×10^{13} cm^{-2} at the surface of In-polar InN films and presented optical data that indicate that the band gap of thick, partially strain-relaxed InN films may be below 0.65 eV.

The authors would like to thank C. G. Van de Walle and D. Segev for useful discussions. This work was supported by DARPA (CNID program) and AFOSR (D. J. Silversmith, program manager).

[1]M. Higashiwaki and T. Matsui, J. Cryst. Growth **269**, 162 (2004).
[2]T. Araki, Y. Saito, T. Yamaguchi, M. Kurouchi, Y. Nanishi, and H. Naoi, J. Vac. Sci. Technol. B **22**, 2139 (2004).
[3]K. M. Yu, Z. Liliental-Weber, W. Walukiewicz, W. Shan, J. W. Ager III, S. X. Li, R. E. Jones, E. E. Haller, H. Lu, and W. J. Schaff, Appl. Phys. Lett. **86**, 071910 (2005).
[4]J. Wu, W. Walukiewicz, K. M. Yu, J. W. Ager III, E. E. Haller, H. Lu, W. J. Schaff, Y. Saito, and Y. Nanishi, Appl. Phys. Lett. **80**, 3967 (2002).
[5]H. Lu, W. J. Schaff, J. Hwang, H. Wu, W. Yeo, A. Pharkya, and L. F. Eastman, Appl. Phys. Lett. **77**, 2548 (2000).
[6]C.-F. S. Chin-An Chang, Nai-Chuan Chen, Pen-Hsiu Chang, and Kuo-Shiun Liu, Phys. Status Solidi C **1**, 2559 (2004).
[7]R. P. T. Craig, H. Swartz, Thomas H. Myers, Hai Lu, and William J. Schaff, Phys. Status Solidi C **2**, 2250 (2005).
[8]F. Chen, A. N. Cartwright, H. Lu, and W. J. Schaff, J. Cryst. Growth **269**, 10 (2004).
[9]V. M. Polyakov and F. Schwierz, Appl. Phys. Lett. **88**, 032101 (2006).
[10]B. Heying, R. Averbeck, L. F. Chen, E. Haus, H. Riechert, and J. S. Speck, J. Appl. Phys. **88**, 1855 (2000).
[11]B. Heying, I. Smorchkova, C. Poblenz, C. Elsass, P. Fini, S. D. Baars, U. Mishra, and J. S. Speck, Appl. Phys. Lett. **77**, 2885 (2000).
[12]H. Lu, W. J. Schaff, J. Hwang, H. Wu, G. Koley, and L. F. Eastman, Appl. Phys. Lett. **79**, 1489 (2001).
[13]Y. Saito, N. Teraguchi, A. Suzuki, T. Araki, and Y. Nanishi, Jpn. J. Appl. Phys., Part 2 **40**, L91 (2001).
[14]H. Ahn, C.-H. Shen, C.-L. Wu, and S. Gwo, Appl. Phys. Lett. **86**, 201905 (2005).
[15]C. J. Lu, L. A. Bendersky, H. Lu, and W. J. Schaff, Appl. Phys. Lett. **83**, 2817 (2003).
[16]C. Adelmann, J. Brault, D. Jalabert, P. Gentile, H. Mariette, G. Mula, and B. Daudin, J. Appl. Phys. **91**, 9638 (2002).
[17]H. Lu, W. J. Schaff, L. F. Eastman, and C. E. Stutz, Appl. Phys. Lett. **82**, 1736 (2003).
[18]T. D. Veal, I. Mahboob, L. F. J. Piper, C. F. McConville, H. Lu, and W. J. Schaff, J. Vac. Sci. Technol. B **22**, 2175 (2004).
[19]C. G. Van de Walle, Phys. Status Solidi B **235**, 89 (2003).
[20]C. Stampfl, C. G. Van de Walle, D. Vogel, P. Kruger, and J. Pollmann, Phys. Rev. B **61**, R7846 (2000).
[21]S.-H. Wei, X. Nie, I. G. Batyrev, and S. B. Zhang, Phys. Rev. B **67**, 165209 (2003).

Downloaded 23 Jul 2006 to 128.111.179.10. Redistribution subject to AIP license or copyright, see http://apl.aip.org/apl/copyright.jsp